

Parallel-plate metamaterials for cloaking structuresMário G. Silveirinha,^{1,2} Andrea Alù,¹ and Nader Engheta^{1,*}¹*Department of Electrical and Systems Engineering, University of Pennsylvania, Philadelphia, Pennsylvania 19104, USA*²*Department of Electrical Engineering-Instituto de Telecomunicações, University of Coimbra, Portugal*

(Received 8 December 2006; published 7 March 2007)

In this work, we assess theoretically the physical response of metamaterial composite structures that emulate the behavior of negative-permittivity materials in certain relevant setups. The metamaterials under analysis consist of metallic parallel-plate implants embedded in a dielectric host in a two-dimensional geometry. Simple design rules and formulas are presented, fully considering the effect and consequences of excitation of higher-order diffraction modes at the metamaterial-dielectric interface. Following the ideas of transparency and cloaking developed by us [Alù and Engheta, *Phys. Rev. E* **72**, 016623 (2005)], we demonstrate, analytically and numerically, that it is possible in this way to design metamaterial cloaks that significantly reduce the total scattering cross section of a given two-dimensional dielectric obstacle in some frequency band. This effect, which may be realized in a feasible way, may find interesting applications in electromagnetic cloaking, total scattering cross section reduction, and noninvasive probing.

DOI: [10.1103/PhysRevE.75.036603](https://doi.org/10.1103/PhysRevE.75.036603)

PACS number(s): 41.20.Jb, 78.66.Sq, 42.50.Gy, 42.70.Qs

I. INTRODUCTION

In recent works, it has been shown that materials with negative permittivity [ϵ -negative (ENG) materials] may have several interesting applications in microwave and optical setups [1–6], and may play an important role in the design of more compact devices or cavities that overcome the diffraction limit [7]. In [8] it was also demonstrated that the peculiar plasmonic resonances responsible for such anomalous properties of ENG materials may be tailored in order to synthesize a dielectric crystal that behaves effectively as a negative-refraction medium, with simultaneously negative permittivity and permeability. Other research groups have exploited the frequency band in which the plasmonic metamaterials have near-zero relative permittivity [ϵ -near-zero (ENZ) materials] to improve the radiation characteristics of antenna setups [9]. ENG or ENZ materials may be effectively employed also to design covers, as cloaks, that drastically reduce the total scattering cross section of a given obstacle, as we showed in [10]. More recently, we also demonstrated that it is possible to squeeze electromagnetic energy through plasmonic subwavelength narrow channels, and that this effect may help reduce the reflectance at a sharp waveguide bend [11].

While these plasmonic materials may be readily available in nature at the infrared (IR) and optical frequencies (e.g., noble metals, polar dielectrics, and some semiconductors [12]), at microwaves this is not the case (except for the plasma below its plasma frequency, of which the ionosphere is an example, having its plasma frequency at microwave frequencies). However, using the metamaterial concept it is possible to construct artificial structures that effectively behave as ENG materials at microwaves [13–16]. In typical designs these composite materials consist of regular arrays of long thin metallic wires that interact with radiation nearly the

same way as an “ideal” ENG material [15], provided that the lattice constant is much smaller than the wavelength of operation.

The aim of this paper is to assess the performance of a specific configuration for synthesizing ENG metamaterials in a setup of practical interest, and at the same time to validate the results of [10] using an artificially made metamaterial. More specifically, following the ideas developed in [10] for transparency and cloaking, here we investigate whether an ENG metamaterial cover consisting of conducting implants at microwave frequencies can be used as a cloak to reduce the specific scattering of a given obstacle at a given microwave frequency range of interest. In [10], it was demonstrated that a proper design of an ideal ENG cover near its plasma resonance may induce transparency, i.e., a dramatic drop in the total scattering cross section of a moderately sized object. In that work, however, ENG materials were assumed to be readily available, which is the case in the IR and visible range of frequencies, but not at lower frequencies. Here we assess whether the same phenomenon may occur using a metamaterial composite cover simulating the behavior of an ENG material.

It is important to note that recently other groups have used alternative strategies to reduce the specific scattering of a given object [17–23], using coordinate transformation techniques and other related concepts that require anisotropic and/or inhomogeneous layers. Also, somehow related with this work, in [24] the concept of hard and soft surfaces was applied in order to reduce the blockage width of cylinders such as struts and masts. It was found that the blockage width of a metal cylinder may be reduced by adding a suitably designed dielectric cover to it, which is consistent with some results reported in this paper. However, the geometry analyzed here is different from the one studied in [24], as well as our perspective and approach to the problem.

Although the most popular ENG metamaterial structure is the wire medium [13–15], we study here the design of covers made of metallic plates [13]. The motivation of our choice is the simplicity of the parallel-plate medium, which consists of a set of waveguides below cutoff. This configuration is rela-

*Author to whom correspondence should be addressed. Email address: engheta@ee.upenn.edu

tively easy to assemble in a practical setup and it further allows relatively uncomplicated numerical and analytical modeling in the two-dimensional (2D) geometry of interest here. We show that, when properly designed, such ENG metamaterials may provide with good approximation the desired electromagnetic response even in complex propagation scenarios. After a discussion on how the interface effects (i.e., the transition from the metamaterial section to another dielectric) can be taken into account and described by effective medium theory, we present some simple design formulas to synthesize such artificial ENG metamaterials. Then we apply these concepts to properly design a metamaterial cover as a cloak that enables the reduction of the total scattering cross section of a given dielectric obstacle, as obtained in [10], and show how the present design is effective for these purposes.

The paper is organized as follows. In Sec. II, we introduce the geometry of the parallel-plate medium, discussing how and under which conditions such a structure can be homogenized, and we establish simple design rules for emulating the response of an ideal ENG slab. In Sec. III, we briefly review the problem of scattering reduction considered here and we find under which conditions it is possible to significantly reduce the total scattering of a given object by designing a proper ENG cover as a cloak. Then we analyze numerically the performance of some design examples, showing how properly designed metamaterial covers may be effective in reducing the cylinder's total scattering cross section. Finally, in Sec. IV we discuss some physical insights and conclusions.

In the following, the time variation $\exp(-i\omega t)$ is assumed.

II. CHARACTERIZATION OF PARALLEL-PLATE ϵ -NEGATIVE METAMATERIALS

A. Parallel-plate medium

More than four decades ago, Rotman [13] proved that a set of parallel plate waveguides below cutoff can simulate an electric plasma at microwave frequencies. Several design techniques were presented in [13], and the concepts were validated experimentally by coating a slot antenna with an artificial plasma-coated cylinder. More recently, the same analogy was explored to simulate the behavior of double-negative media in metallic waveguides [25,26], by loading such waveguides below cutoff with magnetic inclusions. In the following, we briefly discuss the properties and the homogenization of such waveguide-based metamaterials.

The parallel-plate medium under analysis consists of a set of parallel metallic waveguides (see Fig. 1). The distance between the plates is a , and the space between the plates is filled with a nonmagnetic dielectric with relative permittivity ϵ_{diel} . In this work, we assume that the polarization of the fields is such that the electric field is always parallel to the metallic plates (E polarization). As is well known [27], in each waveguide section the electric field can be decomposed into electromagnetic modes with propagation constants:

$$\gamma_n = \sqrt{\left(\frac{\pi}{a}n\right)^2 - \epsilon_{\text{diel}}k_0^2}, \quad n = 1, 2, 3 \dots, \quad (1)$$

where $k_0 = \omega/c$ is the free-space wave number. For long wavelengths the fundamental mode, $n=1$, is dominant. The

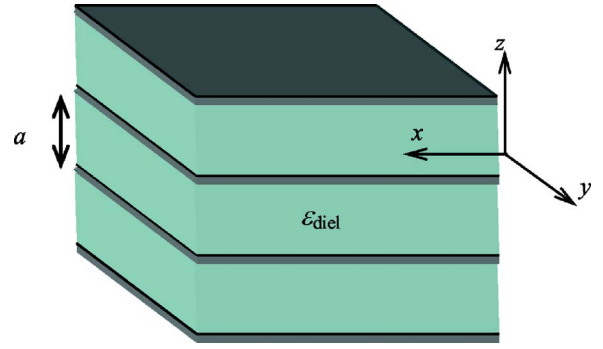


FIG. 1. (Color online) Geometry of the parallel-plate medium as a metamaterial: A periodic set of vanishingly thin metallic plates filled with a dielectric with permittivity ϵ_{diel} .

effective permittivity ϵ_{eff} seen by the fundamental mode (along any direction in the x - y plane) is

$$\frac{\epsilon_{\text{eff}}}{\epsilon_0} = \frac{-\gamma_1^2}{k_0^2} = \epsilon_{\text{diel}} - \frac{\pi^2}{(k_0 a)^2}. \quad (2)$$

Thus the set of metallic parallel plates below cutoff behaves as a lossless electric plasma with a Drude-type model. The effective permittivity of the equivalent medium is negative below the cutoff frequency of the fundamental mode. The plasmalike properties can be controlled by changing the permittivity of the dielectric spacer and the distance between the plates.

The above permittivity model will be proven to be sufficiently accurate for most configurations studied in the present work. Nevertheless, for the sake of completeness and rigor, we must point out that the permittivity model (2) is simplistic and somehow approximate. Indeed, Eq. (2) is only valid for normal incidence. In fact, consider an electromagnetic mode with wave vector component k_z along the z direction. Such a transverse component of the wave vector defines the phase shift of the field from waveguide to waveguide, and it is different from zero for oblique incidence. Since the propagation constant γ_1 of the fundamental mode in the x - y plane directions is independent of k_z , the effective permittivity for an oblique E -polarized wave is given by

$$\frac{\epsilon_{\text{eff}}}{\epsilon_0} = \frac{-\gamma_1^2 + k_z^2}{k_0^2} = \epsilon_{\text{diel}} - \frac{\left(\frac{\pi}{a}\right)^2 - k_z^2}{k_0^2}. \quad (3)$$

Hence the effective permittivity seen by the dominant waveguide mode depends explicitly on k_z as does the equivalent plasma frequency f_p . In particular, f_p decreases as k_z increases, i.e., the plasmalike properties are somehow weaker for oblique incidence. The dependence of the effective permittivity on the wave vector is a manifestation of spatial dispersion [28] which is characteristic of artificial materials with long inclusions [29].

B. Scattering from a set of waveguides below cutoff juxtaposed to a magnetodielectric slab

In order to test the applicability of the permittivity model (3) in a practical setup in which the metamaterial has a finite

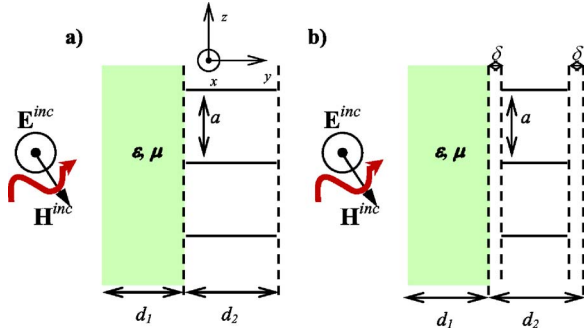


FIG. 2. (Color online) A magnetodielectric slab juxtaposed to metallic waveguides below cutoff. Panel (a): The plates are adjacent to the dielectric slab. Panel (b): Gaps of width δ are placed at the interfaces between the plates and the dielectric and free space.

thickness, we analyze in this section the scattering properties of a system composed of a magnetodielectric slab placed in cascade with such a set of waveguides below cutoff (which is desirably supposed to simulate an ENG material as mentioned in the previous section). The geometry of the structure is depicted in Fig. 2(a), where the magnetodielectric slab is assumed to have relative permittivity ϵ and relative permeability μ . The structure is uniform along the x direction and periodic along the z direction. The width of the dielectric slab and of the waveguides is d_1 and d_2 , respectively.

A TE incident plane wave $\mathbf{E}^{\text{inc}} = E_0 e^{+ik_z z} \hat{\mathbf{u}}_x$, polarized with electric field parallel to the metallic plates illuminates the periodic structure. The incident wave vector is $\mathbf{k}^{\text{inc}} = (0, +i\Gamma_0, k_z)$, where $\Gamma_0 = \sqrt{k_z^2 - k_0^2}$ if $|k_z| > k_0$ and $\Gamma_0 = -i\sqrt{k_0^2 - k_z^2}$ otherwise. The total electric field is the superposition of the incident and scattered waves, i.e., $\mathbf{E} = \mathbf{E}^{\text{inc}} + \mathbf{E}^s$. It is clear that the problem is intrinsically two-dimensional with $\partial/\partial x = 0$ and that the electric field is directed along the x direction everywhere, i.e., $\mathbf{E} = E_x \hat{\mathbf{u}}_x$, satisfying the Helmholtz equation:

$$\nabla \cdot \left(\frac{1}{\mu_r} \nabla E_x \right) + \epsilon_r k_0^2 E_x = 0, \quad (4)$$

where $\epsilon_r(y)$ and $\mu_r(y)$ are the sectionally constant relative permittivity and permeability, respectively. The electric field is continuous in all space, and vanishes at the metallic plates. At the dielectric interfaces $(1/\mu_r)(\partial E_x/\partial y)$ is also continuous. The scattered field $E_x - E_x^{\text{inc}}$, moreover, satisfies Sommerfeld's radiation condition at infinity.

Since the structure is periodic along z , the field can be expanded into Fourier harmonics with propagation constant k_z . For example, inside the dielectric slab the field can be written as

$$E_x = \sum_{n=-\infty}^{\infty} (c_n^+ e^{-\Gamma_n y} + c_n^- e^{+\Gamma_n y}) e^{+i[k_z + (2\pi/a)n]z}, \quad (5)$$

$$\Gamma_n = \sqrt{\left(k_z + \frac{2\pi}{a}n\right)^2 - \epsilon_r \mu_r k_0^2},$$

where c_n^+ and c_n^- are unknown constants. In the free-space region the field can be analogously expanded, by taking into

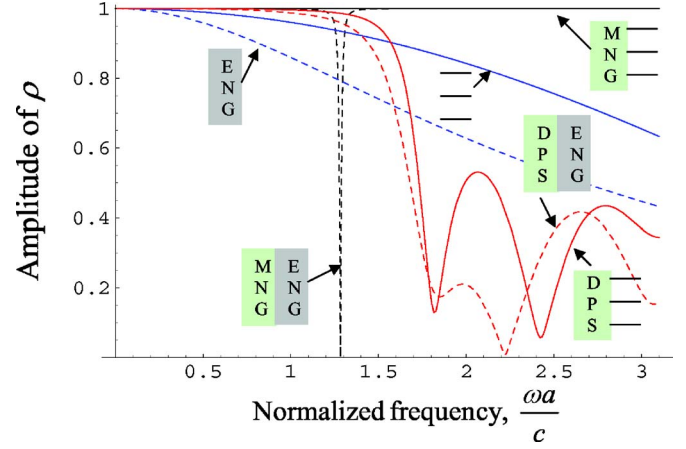


FIG. 3. (Color online) Amplitude of the reflection coefficient as a function of the normalized frequency for different configurations, as indicated schematically in the insets (solid line: Metamaterial configuration; dashed line: Ideal material response): (a) (Blue line—dark in gray scale) ENG slab with thickness $d_2 = 0.3a$. (b) (Red line—light in gray scale) DPS+ENG pair: $d_1 = d_2 = 1.0a$; $\epsilon = 2.0$; $\epsilon_{\text{diel}} = 4.0$. (c) (Black line) MNG+ENG pair: $d_1 = 5.0d_2 = 5.0a$; $\mu = -1/5$; $\epsilon_{\text{diel}} = 1.0$.

account also the radiation condition. On the other hand, inside the metallic plates the field can be decomposed into the waveguide modes described in the previous section. For the waveguide in the interval $0 < z < a$, we can write, for instance,

$$E_x = \sum_{m=1}^{\infty} (b_m^+ e^{-\gamma_m y} + b_m^- e^{+\gamma_m y}) \sin\left(\frac{m\pi}{a}z\right), \quad (6)$$

where b_m^+ and b_m^- are the unknown coefficients of the expansion, and γ_m is given by Eq. (1). Note that outside $0 < z < a$ (unit cell), the field may be obtained from Eq. (6) using Floquet theorem, i.e., exploiting the periodicity of the geometry. The unknown constants may be evaluated by imposing the boundary conditions at the interfaces between the different regions. A mode matching technique [27] may be implemented in order to solve the problem computationally.

As a first example, we investigate the scattering properties of a nonmagnetic dielectric slab, which we refer to in the following as double-positive (DPS) material, with $\epsilon = 2.0$ juxtaposed to a set of parallel plate waveguides embedded in a dielectric with $\epsilon_{\text{diel}} = 4.0$ (i.e., the dielectric material with $\epsilon_{\text{diel}} = 4.0$ fills the space between the metallic plates). The width of the slabs is $d_1 = d_2 = 1.0a$, and the direction of propagation of the incoming wave is along the normal direction. The scattering parameters were computed using the mode matching technique. The electric field was expanded into 26 modes in each region. In Fig. 3 we depict the amplitude of the calculated reflection coefficient as a function of the normalized frequency (solid red line, indicated schematically by the corresponding inset). The corresponding dashed red line represents the response of an ideal ENG material characterized by the permittivity model (3). It is seen that the agreement is in general satisfactory, even though the error for $k_0 a > 1.5$ cannot be considered negligible.

In the second case (blue lines), also plotted in Fig. 3, the DPS slab is removed and the set of waveguides below cutoff is left alone in free space. The width of the metamaterial slab is now reduced to $d_2=0.3a$ and the dielectric between the plates is vacuum with $\epsilon_{\text{diel}}=1.0$. It is seen in Fig. 3 that the deviation between the actual response of the system and the homogenization model becomes very significant. The permittivity model (3) clearly fails to characterize the set of parallel plates below cutoff. At a first glance, a possible explanation of this deviation can be attributed to the width of the waveguides d_2 , which is small compared to the distance between the plates a and, consequently, our metamaterial can hardly be considered a set of parallel plates. The permittivity model given by (3) assumes indeed propagation in a metamaterial that is infinite in the longitudinal (i.e., y axis) direction—a situation that is very different from the one considered in this case. In other words, since the longitudinal width of the metamaterial slab is smaller than the period of the parallel plates, the propagation cannot be accurately described by just the dominant evanescent mode, and the effect of higher order evanescent modes gets more and more important as this longitudinal width becomes comparable with the transverse period. It should be noted that in the application of interest here, i.e., the design of metamaterial covers to reduce the scattering from cylindrical objects as proposed in [10], generally thin layers of metamaterial are required, with thickness being a fraction of the wavelength of operation, implying that the contribution of these higher-order modes will become notably important and should be adequately taken into account.

In order to further study this issue, we analyzed the response of the metamaterial slab when it is paired with a μ -negative (MNG) slab. From [30], we know that the juxtaposition and pairing of ENG and MNG slabs may, under certain conditions, lead to some unusual features, such as resonance, complete tunneling, and zero reflection. For normal incidence, the tunneling conditions that guarantee that the MNG-ENG pair is transparent to radiation are given as (assuming negligible losses) [30]

$$d_{\text{MNG}}\sqrt{\epsilon_{\text{MNG}}|\mu_{\text{MNG}}|} = d_{\text{ENG}}\sqrt{|\epsilon_{\text{ENG}}|\mu_{\text{ENG}}}, \quad (7a)$$

$$\sqrt{\frac{|\mu_{\text{MNG}}|}{\epsilon_{\text{MNG}}}} = \sqrt{\frac{\mu_{\text{ENG}}}{|\epsilon_{\text{ENG}}|}}. \quad (7b)$$

In the above formulas, the subscripts indicate if the material relative parameters ϵ , μ , and thickness d refer to either the ENG or MNG slabs. In the particular case $\epsilon_{\text{MNG}}=\mu_{\text{ENG}}=1.0$, the tunneling condition is equivalent to

$$d_{\text{MNG}} = d_{\text{ENG}}|\epsilon_{\text{ENG}}|, \quad |\mu_{\text{MNG}}||\epsilon_{\text{ENG}}| = 1. \quad (8)$$

We tested if our metamaterial slab can emulate the behavior of an ideal ENG material in such a tunneling scenario. To this end, in this third example, we juxtaposed an ideal MNG slab with permeability $\mu=-1/5$ to a set of parallel plates with $\epsilon_{\text{diel}}=1.0$, and we chose the width of the slabs to be equal to $d_1=5.0d_2=5.0a$ (for simplicity, in this numerical test we neglected the MNG material frequency dispersion). According to Eq. (8), this pair should be transparent to radiation

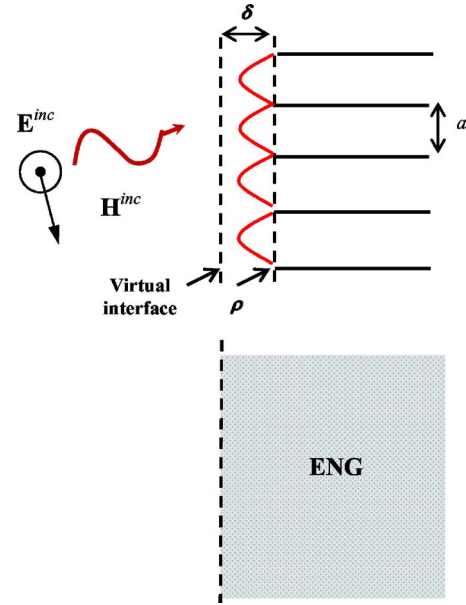


FIG. 4. (Color online) Virtual interface concept: A plane wave with polarization parallel to the metallic plates is scattered by the parallel plate metamaterial (upper panel) in the same way as it would be scattered by an equivalent ENG material (lower panel) with interface displaced a distance δ from the physical interface.

when the effective permittivity of the metamaterial slab is $\epsilon_{\text{eff}}/\epsilon_0=-5$, or equivalently, using Eq. (3), at the normalized frequency $k_0a=1.28$. Disappointingly, the amplitude of the reflection coefficient versus the normalized frequency in this parallel plate case (solid black line in Fig. 3) shows a flat variation over the whole band of interest and no window of tunneling is revealed. The corresponding dashed black line represents, on the other hand, the response of an ideal ENG material following Eq. (3), and consistently with Eq. (8), a sharp dip in the reflection coefficient occurs at $k_0a=1.28$. Thus it is apparent that the set of waveguides below cutoff does not mimic the behavior of an ENG in this resonant configuration, at least as long as the permittivity model represented by Eq. (3) is followed.

What is wrong or incorrect here? Is our model incomplete, or are the observed deviations limitations intrinsic to the metamaterial design in this geometry? In next section we study a canonical problem that may shed some light on these issues.

C. Scattering from a semi-infinite set of waveguides below cutoff

It is clear from the previous section that the permittivity model given by Eq. (3) is unable to accurately describe the actual physical response of the metamaterial slab in relevant configurations. In order to understand such deviation and to quantify the contribution of the higher-order evanescent modes, next we study the reflection of plane waves by a set of semi-infinite waveguides below cutoff.

The geometry is shown in the upper panel of Fig. 4. The material between the waveguide plates is assumed to be free space. This canonical problem was studied many years ago

using the Wiener-Hopf technique [31,32] (see also [27]). It was proved that the reflection coefficient for E -polarized waves at the interface can be written as an infinite product:

$$\rho = -e^{-(\Gamma_0 a/\pi)2 \ln 2} \prod_{n=1}^{\infty} \frac{\gamma_n - \Gamma_0 \Gamma_0 + \Gamma_n \Gamma_0 + \Gamma_{-n}}{\gamma_n + \Gamma_0 \Gamma_0 - \Gamma_n \Gamma_0 - \Gamma_{-n}}, \quad (9)$$

where γ_n is given by Eq. (1) with $\epsilon_{\text{diel}}=1$, and Γ_n is defined as in Eq. (5) with $\epsilon_r=\mu_r=1$. Note that for low frequencies ($k_0 a < \pi$) and paraxial incidence ($k_z \ll k_0$), γ_n and Γ_n are positive numbers for $n \geq 1$ and $n \neq 0$, respectively, while $\Gamma_0 = -i\sqrt{k_0^2 - k_z^2}$ is purely imaginary. Consequently, by direct inspection of Eq. (9) it is clear that $|\rho|=1$, consistently with the fact that the incoming wave cannot transfer power to the set of semi-infinite waveguides below cutoff, as it should happen at the interface between free space and a semi-infinite ENG region.

From Eq. (9) it is also apparent that the effects of the higher-order diffraction modes are expressed by the multiplication factors that involve γ_n (with $n \geq 2$) and Γ_n (with $n \neq 0$), together with the leading exponential parcel. If these terms can be neglected one obtains

$$\rho \approx \rho_h \equiv \frac{\Gamma_0 - \gamma_1}{\Gamma_0 + \gamma_1} \quad (\text{very low frequencies}). \quad (10)$$

Note that ρ_h as defined above is precisely the reflection coefficient for an incident plane wave that impinges on an ideal semi-infinite plasmonic material following the permittivity model (3) (with $\epsilon_{\text{diel}}=1$). Thus all the parcels that were neglected in Eq. (10) are responsible for the deviation between the exact results and the effective medium theory. The physical reason for this inaccuracy is related to the fringe fields at the interface between the metamaterial (formed by stacks of waveguides) and free space, where such higher-order modal contribution is localized. This is also justified by the fact that the electric field profile of the fundamental mode in the metamaterial, and at the interface in particular, is periodic with $\sin[(\pi/a)z]$ distribution at every waveguide section, as illustrated in the upper panel of Fig. 4. On the other hand, in the free-space region the amplitude of the fundamental Floquet harmonic is evidently uniform along z . This implies that the electric field distributions of the fundamental harmonics at the interface are very different in the two media and, as a consequence, evanescent modes that are not taken into account by the homogenization model (3) are necessarily excited at such interface.

In Fig. 5 we depict the phase of the reflection coefficient as a function of the normalized frequency for an E -polarized plane wave incident at $\theta=45^\circ$. Curve (a) represents the approximate effective medium results calculated using Eq. (10), whereas curve (b) represents the exact result calculated with Eq. (9). It is seen that the agreement is reasonable for very long wavelengths, but that the phase difference increases with frequency and it can be as large as 75° or more for $k_0 a \sim \pi$. This may be clearly unacceptable in practical applications. It is possible to evaluate quantitatively the difference between the two approaches, as we do in the following.

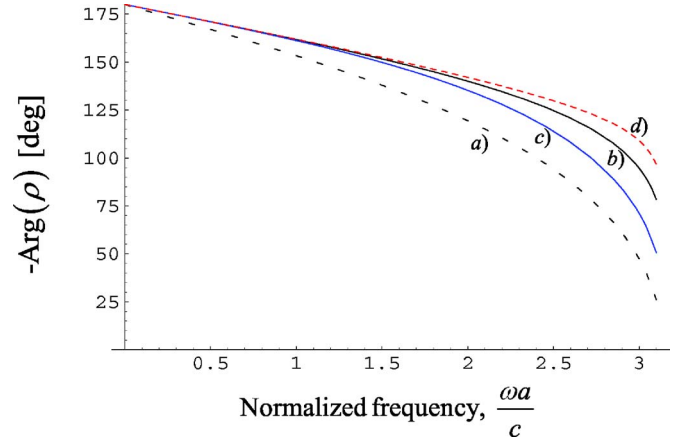


FIG. 5. (Color online) Phase of the reflection coefficient in a semi-infinite parallel plate medium for the angle of incidence $\theta=45^\circ$. (a) Homogenization model without virtual interface. (b) Exact result. (c) Homogenization model with the virtual interface. (d) Homogenization model with the virtual interface calculated with a more accurate formula.

Remembering that Γ_0 is purely imaginary and that γ_n , Γ_n , and Γ_{-n} are real for $n \geq 1$, we find from Eq. (9) that

$$\arg \rho = \arg(\rho_h) + |\Gamma_0| a \frac{2 \ln 2}{\pi} + 2 \sum_{n=2}^{\infty} \arctan\left(\frac{|\Gamma_0|}{\gamma_n}\right) - 2 \sum_{n=1}^{\infty} \left[\arctan\left(\frac{|\Gamma_0|}{\Gamma_n}\right) + \arctan\left(\frac{|\Gamma_0|}{\Gamma_{-n}}\right) \right]. \quad (11)$$

Using the small argument expansion $\arctan(x) \approx x$, and the first order approximations valid for long wavelengths ($k_0 a \ll \pi$ and $|k_z| a \ll \pi$),

$$\frac{|\Gamma_0|}{\gamma_n} \approx \frac{|\Gamma_0| a}{\pi n}, \quad \frac{|\Gamma_0|}{\Gamma_{\pm n}} \approx \frac{|\Gamma_0| a}{2\pi |n|} \quad (n \geq 2), \quad (12)$$

it is found that

$$\delta \equiv -\frac{\arg \rho - \arg(\rho_h)}{2|\Gamma_0|} \approx \frac{1}{\Gamma_1} + \frac{1}{\Gamma_{-1}} - a \frac{\ln 2}{\pi}. \quad (13)$$

Consequently, for long wavelengths we have that

$$\rho = \rho_h e^{+2\Gamma_0 \delta}, \quad (14)$$

which evaluates the difference in the phase of the reflection coefficient between the approximate effective medium model and the exact result. The parameter δ has units of a length and it is dependent on both frequency and wave vector, i.e., $\delta = \delta(k_0, k_z)$. For relatively small frequencies, it is possible to write

$$\delta \approx \delta(k_0 = 0, k_z = 0) \approx a \frac{(1 - \ln 2)}{\pi} \approx 0.1a, \quad (15)$$

where we used Eq. (13) in the second identity. Within this approximation, δ only depends on the spacing between the plates. Interestingly enough, Eq. (14) demonstrates that the phase difference between the exact reflection coefficient and the result predicted by homogenization theory increases lin-

early with $|\Gamma_0|$ under these assumptions, and it is proportional to δ . Moreover, it is evident from the results of Fig. 5 that this phase difference cannot be neglected unless the frequency is very small. In curves (c) and (d) of the same figure, we depict the results predicted by Eq. (14) using δ calculated with Eq. (15) and with the more accurate formula (13), respectively. It is seen that the agreement improves significantly and that the phase difference is kept small for $k_0 a < 2.0$. The important question now is whether we can incorporate the parameter δ into our homogenization model. We investigate this point in the following.

From transmission-line theory it is straightforward to interpret ρ as expressed in Eq. (14) as if the reflection coefficient calculated at the plane $y = -\delta$ would be measured at the physical interface $y = 0$. Therefore, for the incoming wave it looks like the region $y > -\delta$ is filled with an ideal ENG material following the permittivity model (3). This is illustrated in the lower panel of Fig. 4. Thus the plane $y = -\delta$ represents the virtual interface of the equivalent ENG medium. For an external observer the ENG medium starts at this virtual interface rather than at the physical interface of the parallel plate medium. This implies that in the homogenized model the interface with air is not coincident with the physical interface of the metamaterial and this phenomenon is clearly related to the fringe fields associated with the higher-order modes excited at the interface between the parallel-plate medium and the dielectric, as pointed out in a previous paragraph. Sufficiently close to the end of the parallel plates, i.e., in the region $-\delta < y < 0$, we can still experience this fringe field, and that is why heuristically we can justify the extension of the effective ENG material beyond the physical interface of the parallel plates. At the distance δ from them, however, this effect has decayed, and it is not surprising how this distance is proportional to the period between the plates, since the fringe fields are less and less concentrated around the interface when the transverse distance between the plates increases. As discussed before, in the first approximation we can take $\delta \approx 0.1a$, even though strictly speaking the position of the virtual interface δ depends on the frequency and wave vector. The virtual interface concept has also been used in previous works for other metamaterial geometries [33–35].

In order to illustrate the application of this idea, we depict in Fig. 6 the phase of the reflection coefficient as a function of frequency for different angles of incidence. The solid lines represent the exact results, and the dashed lines represent the results calculated using the homogenization model and assuming that the equivalent ENG medium is extended to the virtual interface (using $\delta \approx 0.1a$). As evident from these plots, the general agreement is quite satisfactory, especially for normal incidence and for $k_0 a < 2.0$.

To conclude this section, it is appropriate to point out here that in [13] the fringe field effect was also identified, and it was attributed to the fact that the terminal impedance of a set of waveguides radiating into free space is not coincident with that of the dominant waveguide mode. In order to compensate this mismatch, which is responsible for the inaccuracy of the homogenization model, the terminal impedance of the waveguides was adjusted by adding both dielectric and resistive films to the parallel-plate free-space boundary to compensate, respectively, its susceptance and its conductance.

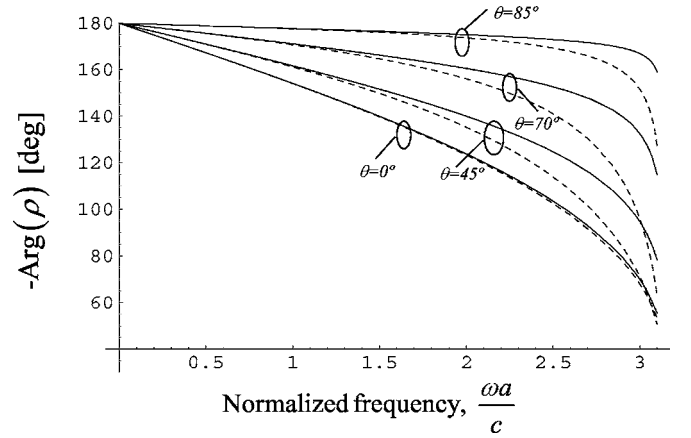


FIG. 6. Phase of the reflection coefficient for a semi-infinite parallel plate medium for incidence along $\theta = 0^\circ, 45^\circ, 70^\circ$, and 85° . Solid lines: Exact result. Dashed lines: Homogenization model with virtual interface (using $\delta \approx 0.1a$).

This procedure has however several limitations, and complicates the actual fabrication of the structure. In the next section, we propose an alternative and simpler approach that is based on the virtual interface concept.

D. Virtual interfaces for finite-width metamaterial slabs

From the study of the canonical problem in the previous section we have learned that for a semi-infinite structure the physical interface is not coincident with the interface of the equivalent ENG medium. Can we use this knowledge to model a finite-width metamaterial slab? Or, in other words, can we design a metamaterial slab that behaves as ENG at given boundaries? It is clear that the physical boundaries of the metamaterial are not coincident with the boundaries of the equivalent ENG material, and that the virtual interfaces should also be considered in this finite-slab case. In fact, the results of the previous section suggest the equivalence shown in Fig. 7. Thus, in order to design an ENG slab that follows the permittivity model (3) and has width d using a parallel plate metamaterial, one should design a parallel-plate system with actual thickness $d - 2\delta$ and, in addition, add two dielectric gaps of thickness $\delta \approx 0.1a$ to the metamaterial on both ends of the slab. The two dielectric gaps should have the same permittivity as the dielectric spacer ϵ_{diel} . In this way the external boundaries of the dielectric gaps become coincident

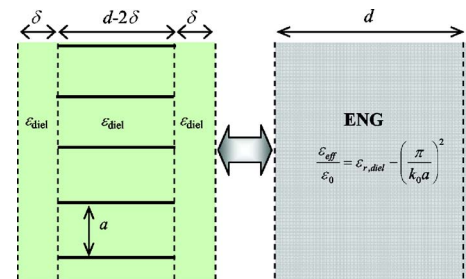


FIG. 7. (Color online) Equivalence between a metamaterial slab with proper virtual interfaces and an ENG medium.

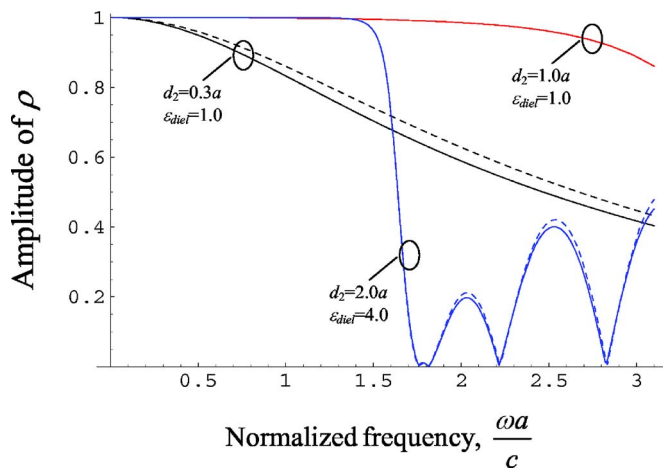


FIG. 8. (Color online) Amplitude of the reflection coefficient as a function of the normalized frequency for different values of the metamaterial slab thickness and of the dielectric filling. The metamaterial slab stands alone in free space. Solid lines: Exact result. Dashed lines: Homogenization theory results taking into account the effect of virtual interfaces. For the case with $d_2=1.0a$, the solid and dashed red lines are practically coincident in the figure.

with the physical interfaces of the equivalent ENG of thickness d . Note that the proposed design rule implies that it is not possible to design an ENG metamaterial with thickness smaller than $d < 2\delta \approx 0.2a$. It is worth noting that a smaller period between the plates makes the homogenization formula given by Eq. (3) more appropriate, since the distance between the inclusions is smaller compared to the wavelength, and in fact the thickness of the required gap becomes shorter. This is associated, however, with a more negative value of effective permittivity, as Eq. (3) shows, since the waveguides are “more” below cutoff.

We now test whether the equivalence suggested in Fig. 7 is correct. To this end, we have calculated the scattering parameters for the modified structure shown in Fig. 2(b) and we have compared the results with homogenization theory. The reflection coefficient data were computed by applying a mode matching algorithm with 26 expansion functions (per section), except in the examples that involve MNG slabs, for which 50 expansion functions (per section) were used to ensure numerical convergence in such resonant configuration. The incoming wave propagates along the normal direction.

In a first example, the metamaterial slab stands alone in free space (i.e., $\epsilon = \mu = 1$ and $d_1 = 0$ in Fig. 2). In Fig. 8 the amplitude of the reflection coefficient is shown for different metamaterial width and ϵ_{diel} values (solid lines), and compared with the results predicted by homogenization theory including the virtual gaps (dashed lines). Remarkably, the agreement is very good over all the frequency range. The only case in which a small difference is noticeable is the one with $d_2=0.3a$ (black lines). For this configuration the width of the metallic plates is only $0.3a - 2\delta = 0.1a$, i.e., the waveguides are very short (their length is the same as their height), and they can arguably be considered metallic strips rather than waveguides. However, even in such a demanding scenario it is seen that our homogenization model describes well the scattering of waves by the structure. Note how the

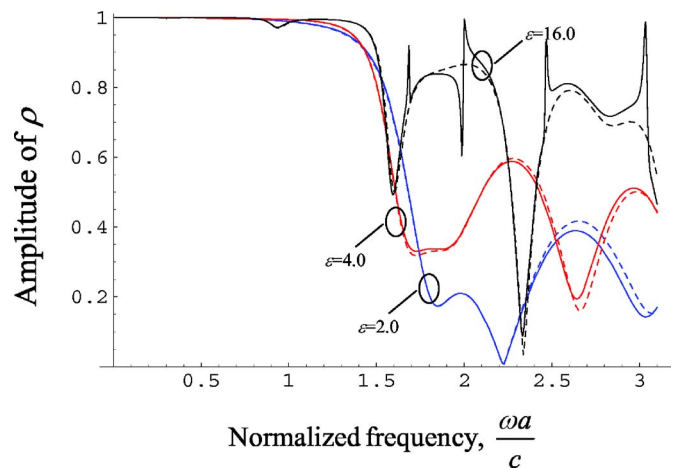


FIG. 9. (Color online) Amplitude of the reflection coefficient as a function of the normalized frequency for different DPS slabs with thickness $d_1=1.0a$. The effective thickness of the metamaterial slab is $d_2=1.0a$ and the permittivity of the dielectric between the metallic plates is $\epsilon_{\text{diel}}=4.0$. Solid lines: Full wave numerical result. Dashed lines: Homogenization theory results taking into account the effect of virtual interfaces.

role of the gaps is essential for the good agreement, comparing these results with those of Fig. 3.

In the next example, reported in Fig. 9, a nonmagnetic DPS slab with thickness $d_1=1.0a$ and varying permittivity ϵ is juxtaposed to a set of parallel plates filled with a dielectric with permittivity $\epsilon_{\text{diel}}=4.0$. The width of the parallel-plate system (including the two dielectric gaps) is $d_2=1.0a$. It is seen that the general agreement is very good in all the cases, even though the effective permittivity of the equivalent metamaterial becomes greater than zero for frequencies close to $k_0 a \sim \pi$.

Next, we assess the performance of the modified metamaterial slab when it is paired with an ideal MNG slab. It was seen in the previous section and in Fig. 3 that, when the gaps were not considered, the tunneling effect could not be observed. Here, we design the metamaterial slab taking into account also the effect of the virtual interfaces. We have analyzed three different configurations: $\mu = -1/9$ and $d_1 = 9.0d_2 = 9.0a$, $\mu = -1/5$ and $d_1 = 5.0d_2 = 5.0a$, and $\mu = -1/2$ and $d_1 = 2.0d_2 = 2.0a$. In all the examples $\epsilon_{\text{diel}} = 1$ and the permittivity of the MNG slab is also unity. As in the previous case, the width d_2 is the sum of the widths of the plates and of the two dielectric gaps. Figure 10 reports the calculated reflection characteristics. The solid lines again correspond to the metamaterial setups, whereas the dashed lines represent the response of the corresponding ENG material obtained following the proposed homogenization model. Consistently with Eq. (8), the reflection characteristic has sharp dips at the frequencies where the tunneling resonant condition is verified. The response of the metamaterial slab compares well with that of the ideal ENG material (especially for the cases $\mu = -1/9$ and $\mu = -1/5$), apart from a slight shift in frequency. For the configuration with $\mu = -1/2$, the agreement is worse and the dip is not as sharp. In general, we verified that the agreement got better when the required effective permittivity of the equivalent ENG was more negative. This

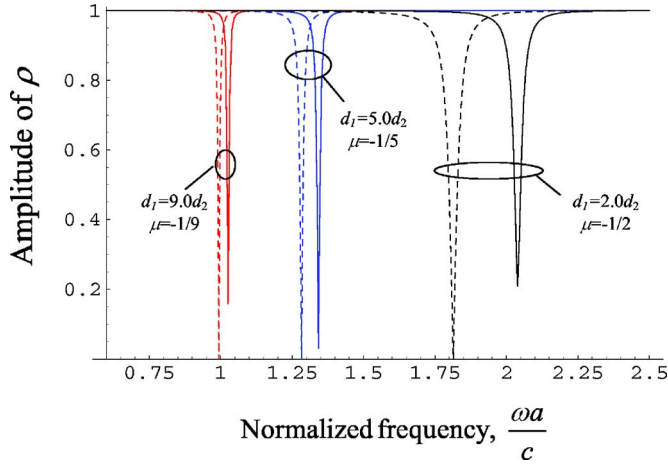


FIG. 10. (Color online) Amplitude of the reflection coefficient as a function of the normalized frequency when the metamaterial slabs are juxtaposed to different MNG slabs. Solid lines: Full wave numerical result. Dashed lines: Homogenization theory results taking into account the effect of virtual interfaces.

is understandable since in these conditions the homogenization theory is expected to be more accurate, because the spacing between the plates is electrically smaller (see also the discussion of [16] in a more general framework). The results of Fig. 10 therefore confirm this trend, remembering that the tunneling effect is observed at the frequency where the effective permittivity of the metamaterial satisfies $|\mu_{\text{MNG}}|\epsilon_{\text{ENG}}=1$ [see Eq. (8)].

The previous examples demonstrate that the modified homogenized model summarized in Fig. 7 can yield very accurate results, even in extremely demanding scenarios, i.e., when the metamaterial slab is paired in a resonant configuration with an MNG slab, or in the case in which the width of the ENG slab is only a fraction of the spacing between the plates, or even when the metamaterial slab has effective permittivity close to or greater than zero. Thus, after this thorough analysis we are ready to assess the performance of this structure in more complicated setups with more practical interest and potential applications.

To conclude this section, we refer that even though the geometry studied here is intrinsically two-dimensional, some of these results may be readily extended to the three-dimensional metamaterial formed by a honeycomb of metallic waveguides with square cross section. Indeed, as pointed out in [36], when a plane wave with electric field parallel to the interface illuminates the honeycomb structure the problem is equivalent to the one studied here (for certain highly symmetric directions). Thus, for the referred polarization, the distance from the virtual interface to the honeycomb structure is again approximately equal to $\delta=0.1a$.

III. REDUCTION OF SCATTERING CROSS SECTION

A. Overview

In [10] it was proven that, under suitable conditions, it is possible to drastically reduce the scattering cross section of spherical and cylindrical objects using lossless plasmonic

covers. As pointed out in [10], this phenomenon can be heuristically understood realizing that an object with permittivity greater than ϵ_0 induces a local electric displacement current that can be antiparallel with the displacement current induced by a (plasmonic) object with permittivity less than ϵ_0 . Thus, if the correct volumetric proportions of materials are put together, the averaged electric displacement current in the combined system object cover may be made very small such that the total electric dipolar radiation from the overall system may become very close to zero. By the same token, even higher order multipole radiation may be cancelled using a similar technique, and therefore with this method the total scattering cross section of moderately sized obstacles with dimensions in the order of half the wavelength of radiation may be drastically lowered [37]. Recently, alternative strategies to reduce the scattering from a given object using metamaterials were proposed in [17–23].

In [10] design formulas that allow the proper dimensioning of the cover material for the case of both spherical and cylindrical objects were derived. Here, we briefly review the theory for the case of cylindrical obstacles. We assume that the fields are E -polarized, i.e., the electric field is parallel to the axis of the cylindrical object. Moreover, all the materials are assumed nonmagnetic.

To begin with, consider the case where the cross section of the obstacle is circular with radius R and when the axis of symmetry is along z . The (relative) permittivity of the obstacle is assumed to be ϵ . We show now that under suitable conditions it is possible to sensibly reduce the total scattering cross section of the object by covering it with a concentric shell with radius R_c made of a material with relative permittivity ϵ_c , under a proper choice of the two parameters of the cover.

The structure is illuminated by a plane wave that propagates along the x direction, with (normalized) electric field polarized along z :

$$\begin{aligned} E_z^{\text{inc}} &= e^{+ik_0x} = \sum_{l=-\infty}^{l=+\infty} i^{|l|} J_{|l|}(k_0r) e^{+il\varphi} \\ &= \sum_{l=0}^{l=+\infty} (2 - \delta_{l,0}) i^l J_l(k_0r) \cos(l\varphi). \end{aligned} \quad (16)$$

In the above, J_l is the J -Bessel function of the first kind and order l , (r, φ) form a system of polar coordinates attached to the center of the dielectric rod, and $\delta_{n,m}$ is the Kronecker delta. By expanding the fields into cylindrical harmonics, it is straightforward to prove that the scattered field can be written as

$$E_z^s = \sum_{l=0}^{l=+\infty} (2 - \delta_{l,0}) i^l c_l H_l^{(1)}(k_0r) \cos(l\varphi), \quad (17)$$

where $H_l^{(1)} = J_l + iY_l$ is the Hankel function of order l , and the coefficients c_l are given by [38]

$$c_l = -\frac{U_l}{U_l + iV_l}, \quad (18)$$

$$U_l = \begin{vmatrix} J_l(kR) & J_l(k_c R) & Y_l(k_c R) & 0 \\ J'_l(kR)k/\mu & J'_l(k_c R)k_c/\mu_c & Y'_l(k_c R)k_c/\mu_c & 0 \\ 0 & J_l(k_c R_c) & Y_l(k_c R_c) & J_l(k_0 R_c) \\ 0 & J'_l(k_c R_c)k_c/\mu_c & Y'_l(k_c R_c)k_c/\mu_c & J'_l(k_0 R_c)k_0/\mu_0 \end{vmatrix}, \quad (19)$$

$$V_l = \begin{vmatrix} J_l(kR) & J_l(k_c R) & Y_l(k_c R) & 0 \\ J'_l(kR)k/\mu & J'_l(k_c R)k_c/\mu_c & Y'_l(k_c R)k_c/\mu_c & 0 \\ 0 & J_l(k_c R_c) & Y_l(k_c R_c) & Y_l(k_0 R_c) \\ 0 & J'_l(k_c R_c)k_c/\mu_c & Y'_l(k_c R_c)k_c/\mu_c & Y'_l(k_0 R_c)k_0/\mu_0 \end{vmatrix}. \quad (20)$$

In the previous equation, $k = k_0 \sqrt{\varepsilon \mu}$ and $k_c = k_0 \sqrt{\varepsilon_c \mu_c}$ are the wave numbers in the dielectric rod and dielectric cover, respectively. As referred above, we assume that the relative permeability of the two materials is unity: $\mu = \mu_c = 1$.

The total scattering cross section per unit length (i.e., total scattering width) of the combined system is given by

$$Q = \frac{4}{k_0} \sum_{l=0}^{l=+\infty} (2 - \delta_{l,0}) |c_l|^2. \quad (21)$$

It can be proven that in the quasistatic limit ($k_0 R_c \ll 1$, $k_c R_c \ll 1$, $k R_c \ll 1$) the scattering coefficients have the asymptotic behavior

$$c_l = o(k_0 R_c)^{2l}, \quad l = 1, 2, \dots, \quad (22)$$

i.e., the coefficients c_l are infinitesimal of order $(k_0 R_c)^{2l}$. On the other hand, for $l=0$, we have that

$$c_0 = \frac{-ik_0^2}{4} [(\varepsilon_c - \varepsilon)\pi R^2 - (\varepsilon_c - 1)\pi R_c^2] + o(k_0 R)^4. \quad (23)$$

Thus, for electrically small obstacles, the terms that contribute more significantly to the scattering cross section are c_0 (associated with the electric dipole moment of the system) and c_1 (associated with its magnetic dipole moment). In general, both coefficients vanish at the same rate, i.e., $(k_0 R_c)^2$, as the frequency decreases. However, when the materials are nonmagnetic ($\mu = \mu_c = 1$), it can be proven that c_1 vanishes at a faster rate, i.e., $(k_0 R_c)^4$, and hence the dominant contribution to the total scattering width is yielded by the electric dipole term c_0 alone. This is the case of interest in this work, when the transverse size of the object is smaller or comparable with about half the wavelength of operation, and the electric dipolar term is dominant over the other scattering terms.

As proven in [10], the specific scattering of the combined system may be made very small in this quasistatic limit if one designs the cover layer in such a way that the contribution of c_0 , and consequently the total electric dipole moment of the covered object, vanishes. From Eq. (23) it is evident that in the static limit such condition is equivalent to

$$0 = (\varepsilon - 1)A + (\varepsilon_c - 1)A_c, \quad (24)$$

where $A = \pi R^2$ and $A_c = \pi(R_c^2 - R^2)$ are the areas of the object and of the cover layer, respectively. Incidentally, it may be rigorously proven that the above formula is valid not only for the geometry under study, but also for arbitrarily shaped cylindrical objects or covers, i.e., the condition in this quasistatic limit for reducing total scattering width is represented by a condition on the ratio between the physical cross sections of the objects and of the cover. This is consistent with the observations made in [10] (see also [39]) that, since the condition is based on the nonresonant phenomenon of the integral cancellation of the induced electric dipole moments, it is little affected by changes in the geometry or small losses. We note that the condition for reduced scattering width (24) implies that, when the permittivity of the object is greater than unity, the required permittivity of the cover needs to be less than unity, i.e., the cover must be made of a plasmonic material, consistent with the results of [10]. To illustrate these concepts we plot in Fig. 11 the total scattering

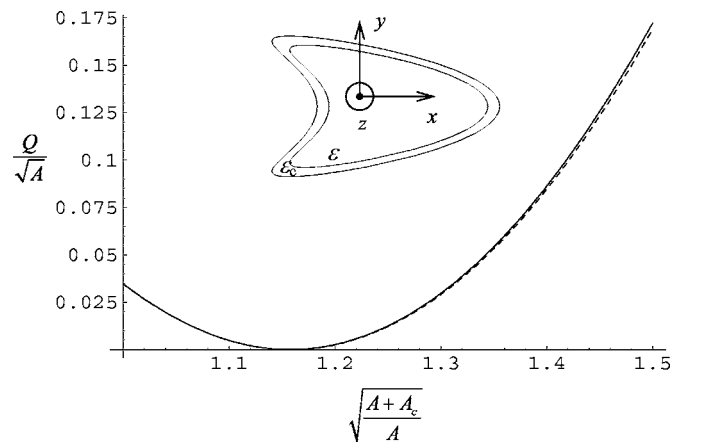


FIG. 11. Normalized scattering width Q for a kite-shaped cylindrical object (as depicted in the inset) as a function of the normalized radius of the plasmonic cover. The permittivity of the object is $\varepsilon=3$ and the one of the cover is $\varepsilon_c=-5$ at the design frequency. Solid line: Incident plane wave propagates along the x direction. Dashed line: Incident plane wave propagates along the y direction. The electric field is polarized along z .

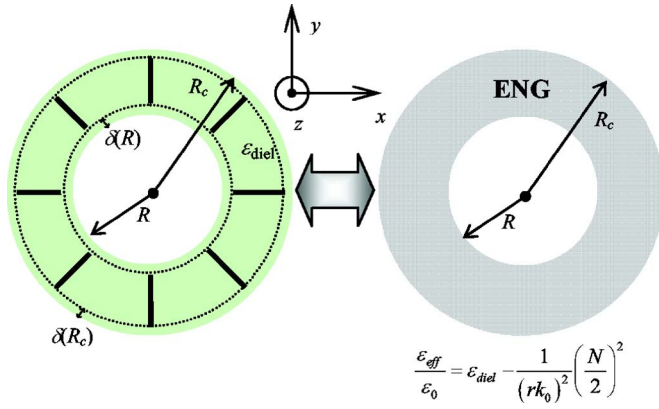


FIG. 12. (Color online) Equivalence between a cylindrical radial-plate metamaterial shell and an ideal ENG cylindrical shell. The analogy is valid as long as the electric field is parallel to the plates, following the results of Sec. II.

width Q for a cylindrical object with kite-shaped cross section and area A . For simplicity, the boundary of the cross section of the cover is nearly parallel to the boundary of the object (the cover is defined mathematically by the Boolean subtraction of the object from an enlarged version of the same object). The area of the cover is A_c . We assumed in the example that the permittivity of the object is $\epsilon=3$ and that the permittivity of the cover is $\epsilon_c=-5$ at the design frequency $k_0\sqrt{A}=0.1\pi$. In Fig. 11 we show Q as a function of the normalized area of the cover. Consistent with Eq. (24), it is seen that Q has a dramatic drop when $\sqrt{(A+A_c)}/A=1.15$, independent of the direction of the incoming wave.

B. Modeling of the metamaterial cover

In the following we apply the concepts explored in the previous section to design an equivalent ENG cover based on the parallel-plate metamaterial configuration. Our previous results and analogies may suggest the equivalence shown in Fig. 12, valid as long as the impinging electric field is along the z direction.

As shown in Fig. 12, the metamaterial shell consists of N metallic plates placed along the directions $\varphi_m=(2\pi/N)m$, with $m=0,1,\dots,N-1$. The angular spacing between the plates is therefore $\Delta\varphi=2\pi/N$. The plates are embedded in a dielectric with permittivity ϵ_{diel} . The structure is uniform along the z direction. Note that there is a gap between the end of the metallic plates and the dielectric interfaces, which, according to the results of the previous section, allows the physical interface of the equivalent ENG shell to coincide with the physical interface of the dielectric shell. The required thickness of the gaps will be discussed in more detail later in this section.

The effective permittivity of the metamaterial cover depicted in the left panel of Fig. 12 may be evaluated extending the result given in Eq. (3) to the case in which the plates are not parallel with each other, but instead are all positioned along the radial direction. In this case clearly the distance between the plates is not constant along the line, but it is a function of the radial distance r , and it is given in particular

by $a(r)=r\Delta\varphi=r2\pi/N$. On the other hand, the phase shift between consecutive plates is related to the azimuthal angular variation of the cylindrical harmonics $\exp(+il\varphi)$, where $l=0,\pm 1,\dots$ is the azimuthal wave number. The phase shift is equal to $k_\varphi a(r)=2\pi l/N$, where k_φ is by definition the azimuthal component of the wave vector in the metamaterial. Replacing a and k_z in Eq. (3), respectively, by $a(r)$ and k_φ , we immediately obtain the following permittivity model for the ENG metamaterial:

$$\frac{\epsilon_{\text{eff}}}{\epsilon_0} = \epsilon_{\text{diel}} - \frac{\left(\frac{N}{2}\right)^2 - l^2}{(k_0 r)^2}. \quad (25)$$

Thus the effective permittivity of the metamaterial shell becomes a function of the radial distance, i.e., the medium is inhomogeneous, as expected, since the distance between the metallic plates is not kept constant. Also, it is seen from Eq. (25) that the plasma frequency of the equivalent medium depends both on the number of implants N and on the azimuthal number l . This latter dependence of the effective permittivity on the azimuthal variation of the field is once again a manifestation of the spatial dispersion of the cover. We have shown in Sec. II how the effective permittivity of a set of parallel plates depends on the wave vector component k_z , implying that the effective permittivity seen by the external field depends not only on the frequency but also on the *direction of incidence* of the impinging field. Here for the metamaterial shell depicted in Fig. 12 the situation is analogous: Not only does the effective permittivity seen by the impressed field depend on frequency, but also on the *azimuthal variation* of the field. In other words, incoming waves with different azimuthal variations “see” a medium with a different effective permittivity. All these unusual phenomena are a manifestation of strong spatial dispersion, which is the price we have to pay for using such a relatively simple (but still very effective) geometry for obtaining an equivalent ENG material.

Another important aspect is the effect of the fringe fields and the dimensioning of the dielectric gaps for the virtual interfaces, particularly due to the sensitivity of the design and the thin dimensions of the required cover. In Sec. II it has been established that the thickness of the dielectric gaps should be approximately equal to $\delta=0.1a$. In this cylindrical configuration (Fig. 12), since the distance between the plates is not uniform $a=a(r)$, the required thickness for the dielectric gaps should also depend on the distance from the origin:

$$\delta(r) \approx 0.1 \frac{2\pi}{N} r. \quad (26)$$

For instance, suppose we want to design an ENG cylindrical shell in the region $R < r < R_c$ following the permittivity model (25). The equivalent metamaterial structure should therefore consist of a dielectric shell with permittivity ϵ_{diel} defined over the region $R < r < R_c$, and of N metallic implants extending in the range $R + \delta(R) < r < R_c - \delta(R_c)$. This equivalence is depicted in Fig. 12.

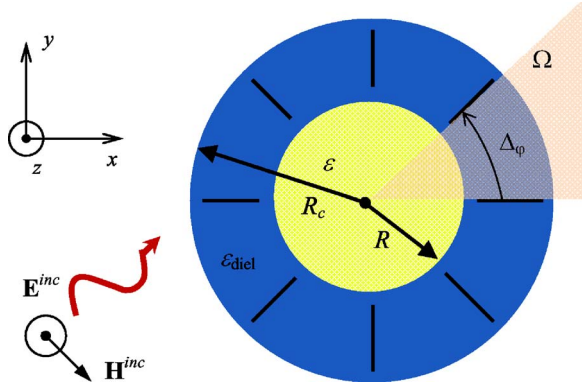


FIG. 13. (Color online) Geometry under analysis: A dielectric cylinder covered with a radial-plate metamaterial consisting of conducting implants embedded in a dielectric shell. The unit cell Ω is shown.

C. Mode matching solution

Once the “radial-plate” metamaterial shell has been characterized, we are ready to assess its performance in the scattering problem. The idea is to cover a dielectric object with permittivity ε with a properly designed metamaterial shell, so that the total scattering width of the combined objects is reduced when compared with the scattering width of the uncovered cylinder. The geometry of the structure is shown in Fig. 13. The system is supposed to be illuminated by a plane wave with electric field polarized along the cylinder axis.

In order to compare the simple effective medium model, as represented by Eq. (25), with the actual physical behavior of the metamaterial shell, here we apply a mode matching technique that solves rigorously the electromagnetic problem of Fig. 13. Expanding the incident plane wave into cylindrical harmonics (16) of the form

$$\psi_l^{\text{inc}} = i^{|l|} J_{|l|}(k_0 r) e^{il\varphi}, \quad l = 0, \pm 1, \pm 2, \dots, \quad (27)$$

it is sufficient to solve the problem independently for each generic cylindrical harmonic ψ_l^{inc} , owing to the linearity of the problem and the superposition principle.

Let ψ be the total electric field (polarized along z) over the entire space, induced by the cylindrical harmonic ψ_l^{inc} . The incident field satisfies the Floquet property $\psi_l^{\text{inc}}(r, \varphi + \Delta_\varphi) = \psi_l^{\text{inc}}(r, \varphi) e^{il\Delta_\varphi}$. Since the implants are uniformly spaced and directed along the radial direction, the whole structure is also invariant to a rotation $\Delta_\varphi = 2\pi/N$ with respect to the axis of symmetry and, thus, also the total field satisfies the Floquet condition as well:

$$\psi(r, \varphi + \Delta_\varphi) = \psi(r, \varphi) e^{il\Delta_\varphi}. \quad (28)$$

This implies that the electromagnetic field over all space is determined once the field in the angular sector (of the x - y plane) $\Omega = \{(r \cos \varphi, r \sin \varphi) : 0 < \varphi < \Delta_\varphi, r > 0\}$ is found. In other words, Ω , as depicted in Fig. 13, can be regarded as the unit cell of the system.

From Eq. (28) we can deduce that $\psi(r, \varphi) e^{-il\varphi}$ is periodic with period $\Delta_\varphi = 2\pi/N$, and therefore for $r > R_c$ the total field can be expanded into

$$\psi = \psi_l^{\text{inc}} + \sum_{n=-\infty}^{+\infty} b_n^{\text{ext}} H_{|l+nN|}^{(1)}(k_0 r) e^{i(l+nN)\varphi}, \quad r > R_c, \quad (29)$$

where b_n^{ext} are unknown expansion coefficients. Inside the dielectric cylinder, we can write as well

$$\psi = \sum_{n=-\infty}^{+\infty} a_n^{\text{obj}} J_{|l+nN|}(kr) e^{i(l+nN)\varphi}, \quad 0 \leq r < R, \quad (30)$$

where $k = k_0 \sqrt{\varepsilon \mu}$ is the wave number inside the dielectric object and a_n^{obj} are unknown coefficients. Similarly, in the dielectric gaps $R < r < R + \delta(R)$ and $R_c - \delta(R_c) < r < R_c$, the field can be expanded into

$$\psi = \sum_{n=-\infty}^{+\infty} [a_n^{\text{gap},j} J_{|l+nN|}(k_{\text{diel}} r) + b_n^{\text{gap},j} Y_{|l+nN|}(k_{\text{diel}} r)] e^{i(l+nN)\varphi}, \quad (31)$$

where the unknowns are $a_n^{\text{gap},j}$ and $b_n^{\text{gap},j}$ ($j=1,2$), and $k_{\text{diel}} = k_0 \sqrt{\varepsilon_{\text{diel}} \mu}$ is the wave number in the dielectric host. Finally, inside the waveguide plate region $R + \delta(R) < r < R_c - \delta(R_c)$, ψ must vanish at $\varphi=0$ and $\varphi=\Delta_\varphi$ because of the boundary conditions on the conducting plates. Therefore, in this region, we have

$$\psi = \sum_{m=1}^{+\infty} [a_m^{\text{wg}} J_{mN/2}(k_{\text{diel}} r) + b_m^{\text{wg}} Y_{mN/2}(k_{\text{diel}} r)] \sin\left(\frac{mN}{2} \theta\right), \quad (32)$$

$$R + \delta(R) < r < R_c - \delta(R_c), \quad 0 < \varphi < \Delta_\varphi,$$

where a_m^{wg} and b_m^{wg} are the unknown amplitudes. It is worth noting that in this case, even though the metallic plates delimit the propagation region, the variation of the field with r does not decay exponentially in this region. The reason is that, since the spacing between the plates is not uniform, there is no cutoff frequency for an infinitely extended metallic sector.

The unknown coefficients are calculated by matching the fields at the $r=\text{const}$ interfaces. More specifically, imposing that ψ and $\partial\psi/\partial r$ are continuous (we underline again that the relative permeability is assumed to be unity everywhere) the expansion coefficients in all the regions may be found numerically using the mode matching algorithm.

The scattering cross section per unit length (i.e., scattering width) Q of the system is then readily calculated from the power density scattered by all the incident harmonics divided by the intensity of the incident Poynting vector. We find

$$Q = \frac{4}{k_0} \sum_{l=-\infty}^{l=+\infty} |b_{l,\text{tot}}^{\text{ext}}|^2, \quad b_{l,\text{tot}}^{\text{ext}} = \sum_{q=-\infty}^{\infty} b_{-q}^{\text{ext},(l+qN)}. \quad (33)$$

Here $b_n^{\text{ext},(l)}$ represent the coefficients b_n^{ext} in Eq. (29), with the superscript l to explicitly indicate that these coefficients are calculated for the cylindrical harmonic ψ_l^{inc} .

It is interesting to note that if the dielectrics gaps can be ignored and the fundamental mode [i.e., the mode with $m=1$ in Eq. (32)] inside the metallic plate region is sufficient to accurately describe the wave propagation, then it is straightforward to verify that the average field

$$\psi_{\text{av}}(r) = \frac{1}{\Delta_\varphi} \int_0^{\Delta_\varphi} \psi(r, \varphi) e^{-il\varphi} d\varphi \quad (34)$$

satisfies the wave equation

$$\frac{1}{r} \frac{\partial}{\partial r} \left(r \frac{\partial \psi_{\text{av}}}{\partial r} \right) - \frac{l^2}{r^2} \psi_{\text{av}} + k_0^2 \varepsilon(r) \psi_{\text{av}} = 0, \quad (35)$$

where $\varepsilon(r) = \varepsilon_{\text{eff}}/\varepsilon_0$ is given by Eq. (25) inside the metamaterial and by the relative permittivity of the structure in the remaining regions. In other words, under the previous hypothesis the metamaterial behaves indeed as an effective material with permittivity given by Eq. (25). This simple result further supports the present homogenization model, even though, following the results of Sec. II, we expect the higher-order diffraction modes to be non-negligible when a finite shell is considered, and that they should be properly taken into account by introducing suitable dielectric gaps as indicated by Eq. (26).

D. Reducing scattering width of dielectric cylinders using an ENG metamaterial cover

Following the theory for synthesizing and homogenizing a cylindrical radial-plate metamaterial, we present next a specific design example for reduction of total scattering width. We still have to deal with a minor problem. Indeed, in Sec. III A it was assumed that the plasmonic material is uniform, while the permittivity of the metamaterial given by Eq. (25) depends on r . This is not necessarily inconvenient, but it may make more difficult the design of the cover for the effect predicted in [10]. However, since the thickness of the required metamaterial cover shell is generally thin, Eq. (25) can be approximated by its spatial average over $R < r < R_c$:

$$\frac{\varepsilon_{\text{eff}}}{\varepsilon_0} \approx \varepsilon_{\text{diel}} - \frac{\left(\frac{N}{2}\right)^2}{k_0^2 R R_c}, \quad R < r < R_c. \quad (36)$$

We will use this formula to design the metamaterial cover.

In our first example, a dielectric cylinder with permittivity $\varepsilon=3$ and radius R is considered. Suppose that we want to reduce the total scattering width of this cylinder at the normalized frequency $k_0 R = 0.8$ (i.e., when the free-space wavelength is $\lambda_0 = 3.9 \times 2R$) using a plasmonic material with permittivity $\varepsilon_c = -3$. As discussed in Sec. III A and in [10], the dominant contribution to the total scattering cross section under these conditions is mainly represented by the electric dipole moment radiation. This contribution may be made very small by choosing the radius R_c of the cover in such a way that the expression for c_0 , as given by Eq. (18), yields zero at the frequency of interest. Alternatively, we can dimension R_c so that the total scattering width Q given by Eq. (21) becomes sufficiently small. We chose this latter alternative, and found that $R_c = 1.43R$ is a good value for obtaining the desired effect. Note that the approximate condition (24) would yield a different value for R_c , since it is accurate only in the static limit, whereas in this example the wavelength inside the dielectric object is comparable with its physical size.

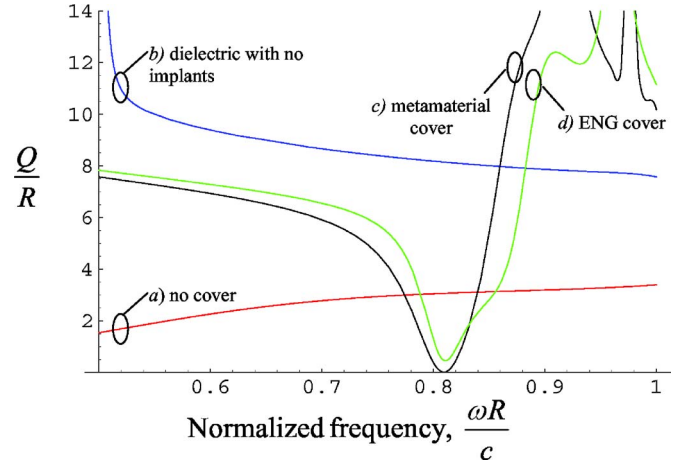


FIG. 14. (Color online) Normalized scattering width as a function of the normalized frequency. (a) Cylindrical dielectric object with permittivity $\varepsilon=3$ and radius R , with no cover around it. (b) Object covered with dielectric shell with $\varepsilon=35.4$. (c) Object covered with metamaterial (dielectric shell+12 implants). (d) Ideal ENG cover following the Drude model (36).

To dimension the metamaterial cover we use $l=0$ in Eq. (36) (since, as noticed above, c_0 is the dominant contribution to Q), and we solve the equation $\varepsilon_{\text{eff}}/\varepsilon_0 \approx \varepsilon_c$ for $\varepsilon_{\text{diel}}$. We still have a degree of freedom for the number of metallic implants N . This number cannot be too large, since otherwise the required permittivity $\varepsilon_{\text{diel}}$ for the dielectric host gets very large as well, and this is not recommended for practical reasons due to the inevitable presence of losses in high-index materials. On the other hand, the number of implants cannot be chosen too small, since otherwise the homogenization model loses its validity.

In the first example, we use $N=12$, requiring $\varepsilon_{\text{diel}}=35.4$. The thickness of the dielectric gaps is $\delta(R)=0.05R$ and $\delta(R_c)=0.07R$. Figure 14 reports the total scattering cross section per unit length as a function of the normalized frequency. When the dielectric object stands alone in free space with no cover [curve (a)] the corresponding scattering width is characterized by a relatively slow growth with frequency, as it is generally expected. When the object is covered with a shell of permittivity $\varepsilon_{\text{diel}}=35.4$ without the metallic implants [curve (b)] the scattering width increases considerably, as justified by the corresponding increase in the physical cross section of the object. However, when this same dielectric shell is loaded with 12 metallic implants [curve (c)], as proposed in Fig. 13, the scattering width dramatically drops at the design frequency, consistent with the previous theoretical considerations. For the purpose of comparison, we plot in curve (d) the scattering width that the object would have when covered with an ideal ENG material following the Drude type model (36). It is seen that these two lines follow qualitatively the same trend, demonstrating how, notwithstanding the many approximations considered in the homogenization process, our formalism and theory are applicable. It is worth underlining how the results obtained with the metamaterial shell are even slightly better than those expected when an ideal plasmonic cover is employed.

If the number of implants is reduced the results remain exciting, as Fig. 15 and Fig. 16 show, referring respectively

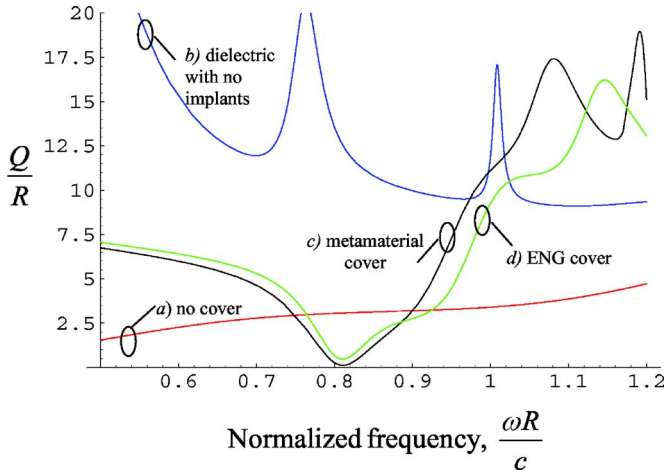


FIG. 15. (Color online) Similar to Fig. 14, but for eight implants: Normalized scattering width as a function of the normalized frequency. (a) Cylindrical dielectric object with no cover. (b) Object covered with a dielectric shell with $\epsilon=14.1$. (c) Object covered with metamaterial (dielectric shell+eight implants). (d) ideal ENG cover following the Drude model (36).

to the case of $N=8$ and $N=4$. For $N=8$ we obtain $\epsilon_{\text{diel}}=14.1$, $\delta(R)=0.08R$, and $\delta(R_c)=0.11R$, and for $N=4$ we obtain $\epsilon_{\text{diel}}=1.26$, $\delta(R)=0.16R$, and $\delta(R_c)=0.22R$. It is interesting to note that, for design purposes, ϵ_{diel} varies with N^2 . For $N=8$ (Fig. 15) the results are qualitatively similar to those of the previous example, except that the frequency bandwidth over which the phenomenon of reduction of scattering occurs has increased (notice how, as already underlined in the previous lines, this effect does not rely on any specific resonance between the two utilized materials, and therefore in all these examples the reduction of scattering cross section has a relatively smooth variation with frequency). On the other hand, for $N=4$ (Fig. 16) some stronger disagreement be-

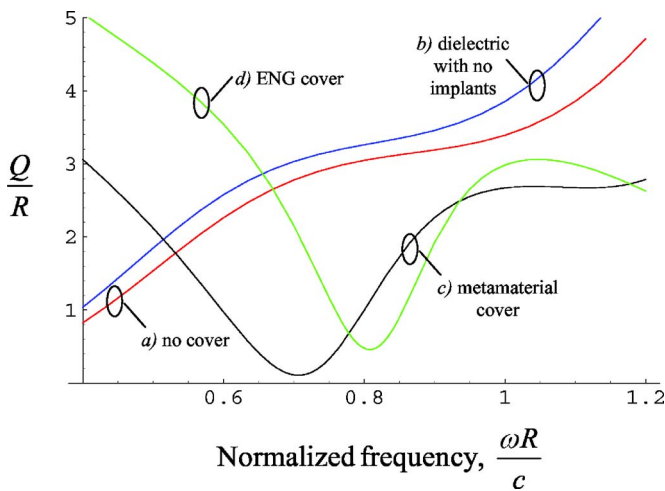


FIG. 16. (Color online) Similar to Fig. 14 and Fig. 15, but for four implants: Normalized scattering width as a function of the normalized frequency. (a) Object with no cover. (b) Object covered with dielectric with $\epsilon=1.26$. (c) Object covered with metamaterial (dielectric+four implants). (d) Ideal ENG cover following the Drude model (36).

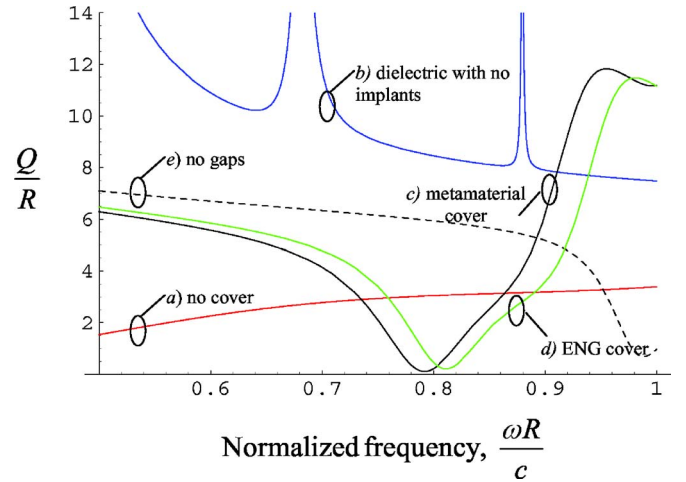


FIG. 17. (Color online) The effect of the virtual interface: Normalized scattering width as a function of the normalized frequency. (a) Cylindrical dielectric object with no cover. (b) Object covered with a dielectric shell with $\epsilon=38.8$. (c) Object covered with metamaterial (dielectric shell+12 implants). (d) Ideal ENG cover following the Drude model (36). (e) Object covered with metamaterial with no gaps.

tween the effective permittivity model and the actual metamaterial design is noticeable. The reason is clearly associated with the fact that for such a small number of implants, adjacent metallic plates are not nearly parallel to each other (in this case of $N=4$ they are even perpendicular to each other), and so the homogenization model tends to fail (still the agreement between the curves is fairly good). Also note that in this case, due to the increased thickness of the dielectric gaps, the length of the plates is only $0.05R$.

In the last example reported in Fig. 17, we consider the same dielectric object as in the previous cases, but we fix now the radius of the cover to be $R_c=1.2R$ (the thickness is reduced to less than half with respect to the previous examples), and we evaluate the required value of permittivity of the cover for reducing the scattering cross section at the design frequency. We find that in this case $\epsilon_c=-6.9$ is a good choice. Fixing $N=12$ we get from the previous formulas $\epsilon_{\text{diel}}=38.8$, $\delta(R)=0.05R$, and $\delta(R_c)=0.06R$. As seen in Fig. 17, apart from a small shift in frequency, the metamaterial cover response [curve (c)] compares well with the homogenization model [curve (d)]. We also show in curve (e) the response of the metamaterial cover when the cover is the same as in curve (c), but the dielectric gaps are removed and the implants start at the physical boundary of the dielectric region. It is seen that the window of scattering reduction is not obtained in this case, underlining the relevance and importance of the virtual interface concepts in the design of such thin metamaterial shells. This further confirms the results of this work in the design of metamaterials based on the parallel plate medium configuration.

Owing to the absence of the resonance in this phenomenon, as already underlined, we stress here how these results are not sharply depending on the symmetric shape of the object or on the geometrical parameters of the design, but

they may be obtained also after small variations of their values.

E. Finite-integration-technique numerical solution

In order to further confirm the feasibility of this technique to reduce the scattering width of cylindrical objects, and to better underline the physics of the phenomenon, in this section we report some full-wave numerical simulations, obtained with a finite-integration-technique commercial software [40], of the structure of Fig. 14, i.e., a dielectric cylinder with $\epsilon=3$ and $k_0R=0.8$, surrounded by a parallel-plate metamaterial with $N=12$ and $\epsilon_{\text{diel}}=35.4$. These numerical simulations agree very well with our predictions of Fig. 14 on the reduction of the scattering width at the design frequency. Here we report the near-field and far-field distributions at this frequency, in order to understand the electromagnetic behavior of this setup.

In particular, Fig. 18 shows the electric near-field amplitude for the three cases of (a) the dielectric cylinder surrounded by the cover as designed in Fig. 14, (b) the same geometry, but with the metallic plates removed, and (c) the same geometry, but with the metallic plates extended also inside the virtual interface regions. In the three cases the structure is excited by a plane wave impinging from the right of the figure with electric field amplitude equal to 1 V/m. It is noticeable how the presence of the metallic plates, properly designed as in Fig. 18(a), drastically reduces the total perturbation of the plane-wave field from the cylindrical system and the field is almost uniform even in the very near field of the structure. Only inside the cover is a strong perturbation of the field around the metallic plates visible, as expected. It is also evident from this figure how the proper design of the gaps for the virtual interface is necessary to obtain the desired scattering reduction. When the gaps are not present, in fact, as in Fig. 18(c), the perturbation of the field distribution is much larger in all directions. Also the absence of the metallic plates, as in Fig. 18(b), shows a strong perturbation of the impinging field.

Figure 19 shows the power flow distribution for the same three cases, showing evidently how the plane wave impinging on the properly covered cylinder [Fig. 19(a)] tunnels through the system as if the object were not present, even in the very near field of the surface of the cover. The figure shows also how the anomalous tunneling takes place inside the cover, where the proper design of the metallic plates in Fig. 19(a) allows the redirection of the power flow distribution to mimic the absence of the system. In Fig. 19(b) and Fig. 19(c) this behavior, as expected, is not achieved and the plane wave power flow is strongly perturbed by the object with a relatively large shadow region induced on the back of the covered cylinder.

Figure 20, finally, shows the far-field radiation patterns for the three cases. The drastic reduction of radiated power is noticeable, at every angle and in total, for the case of Fig. 20(a). Consider also that the scale in Fig. 20(a) is much reduced with respect to the other two cases. Our technique proves to drastically reduce the total scattering width of the object in the very near as well as far field.

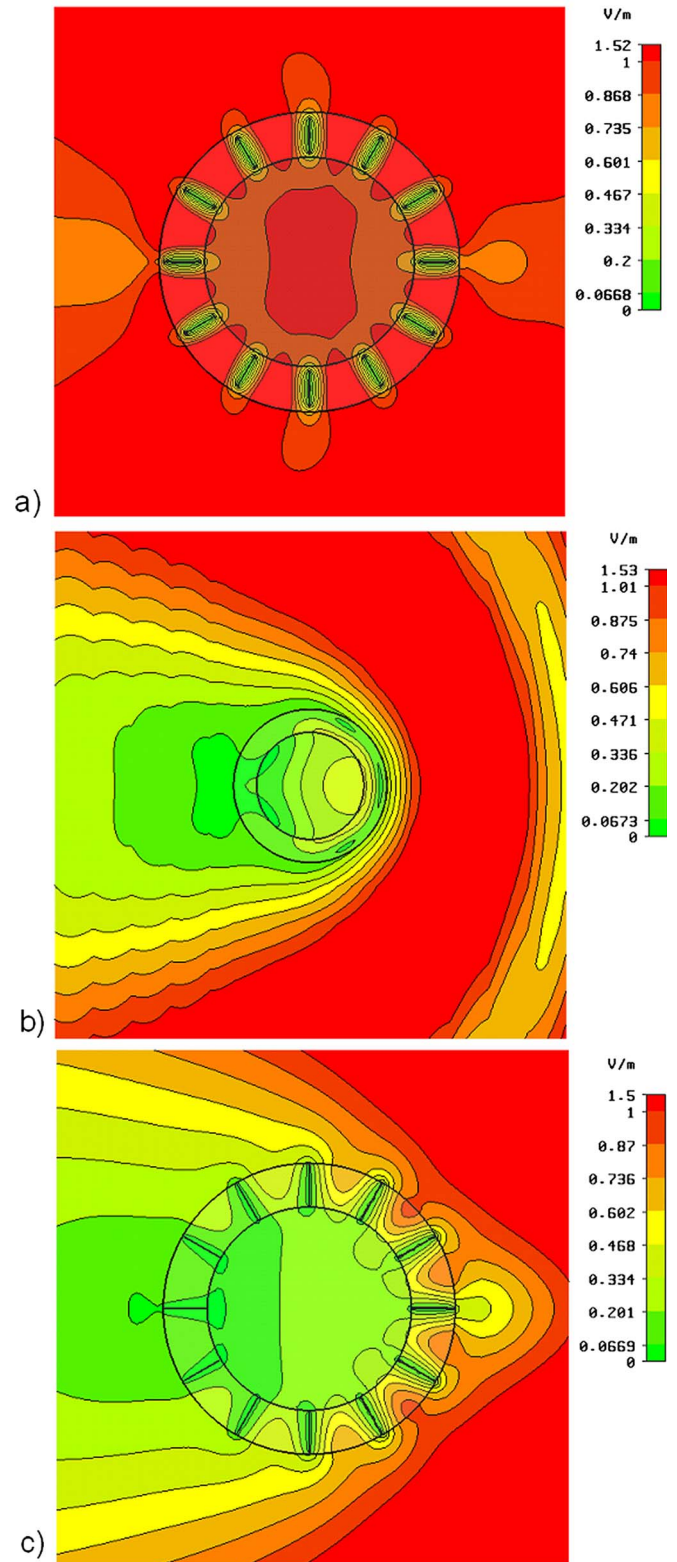


FIG. 18. (Color online) Electric field amplitude for the case of Fig. 14 at the frequency for which $k_0R=0.8$ in the three cases of (a) with cover designed as in Fig. 14, (b) with the same cover, but removing the metallic plates, and (c) again with the same cover, but with metallic plates extended also in the virtual interface.

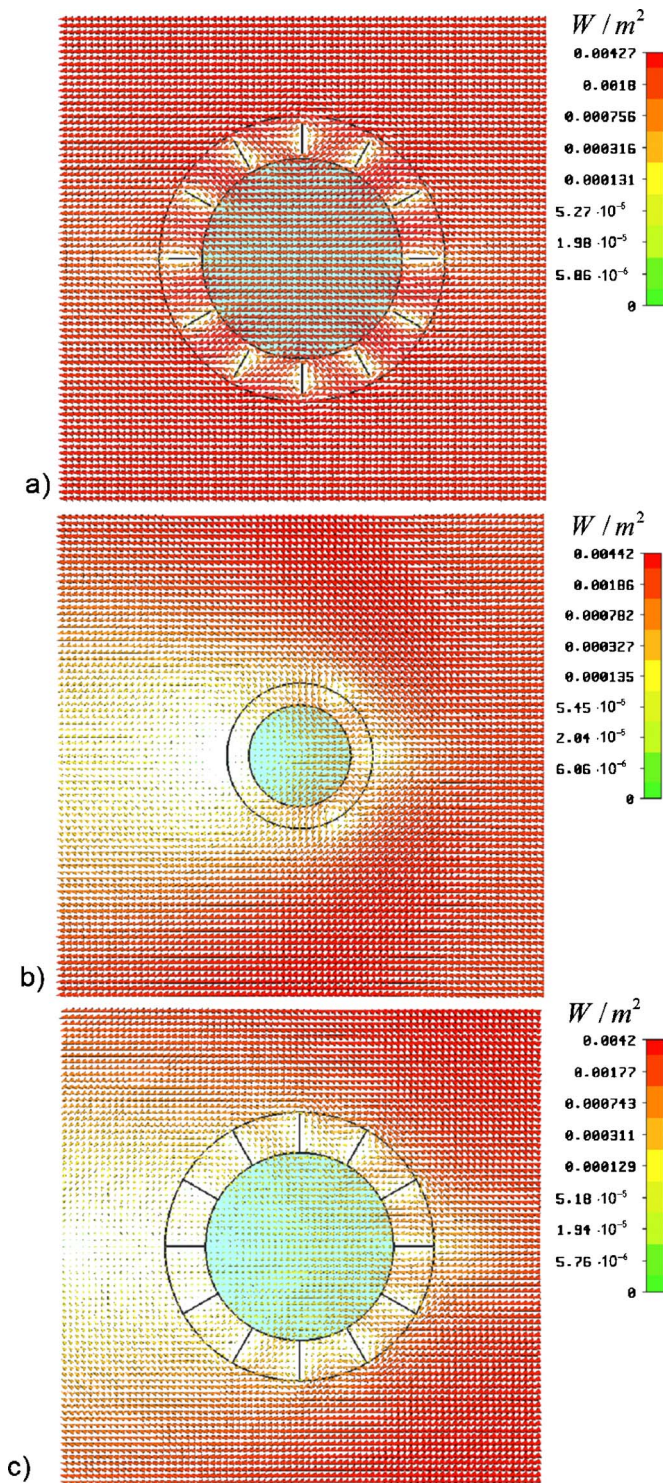


FIG. 19. (Color online) Power flow (real part of the Poynting vector) in the three cases of Fig. 18.

IV. CONCLUSIONS

In this work, we have presented the homogenization and design of artificial materials that consist of a set of metallic waveguides below cutoff. We have shown that even in simple propagation scenarios a dominant mode description of the artificial medium is insufficient to accurately describe

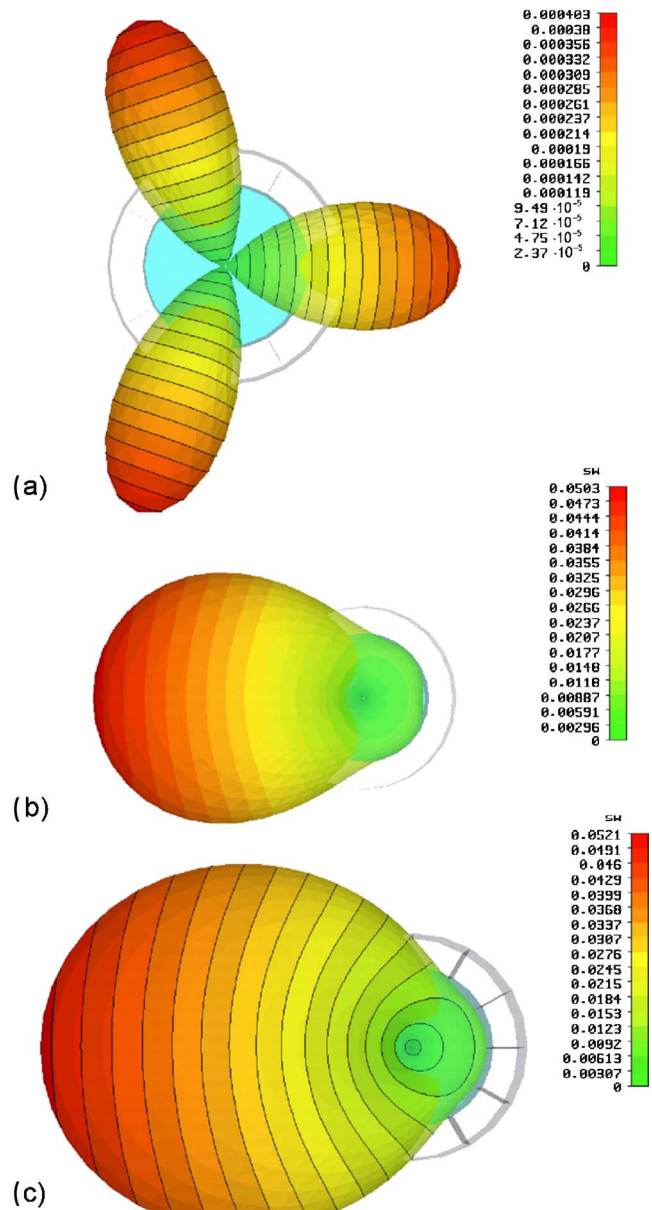


FIG. 20. (Color online) Far-field radiation patterns in the three cases of Fig. 18 [notice how in (a) the scale is different, and much lower, with respect to the other cases].

the electrodynamics of the structure because of the effect of higher-order diffraction modes excited at the entrance and/or exit interface of the metamaterial. It has also been shown that the physical interface of the structure is not coincident with the virtual interface of the homogenized model and therefore it is necessary to introduce dielectric gaps near such interfaces to accurately design ENG metamaterials in this configuration. In order to test our design formulas in an interesting propagation scenario, we have investigated analytically and numerically whether the metamaterial could be employed as a cover in order to reduce the total scattering cross section of 2D dielectric objects, following the theoretical results reported in [10]. It has been demonstrated that, if the parallel-plate metamaterial shell is properly designed, the

behavior and effect of the cover are completely consistent with the theoretical results derived in [10], and in particular such metamaterial covers may provide scattering reduction for the combined object-cover system. The generalization of the results to the case in which the metallic implants are not

perfectly conducting, but rather are plasmonic themselves (which is the case when metallic implants are considered at infrared or optical frequencies), is currently underway. This may be an exciting extension of the current results at higher frequencies and it will be the topic of a future publication.

-
- [1] *Metamaterials—Physics and Engineering Explorations*, edited by N. Engheta and R. W. Ziolkowski (IEEE Press, John Wiley&Sons, New York, 2006).
- [2] *Metamaterials*, edited by R. W. Ziolkowski and N. Engheta, special issue of IEEE Trans. Antennas Propag. **51**(10), (2003).
- [3] *Negative Refraction and Metamaterials*, edited by J. B. Pendry, focus issue of Opt. Express **11**(7), 639–760 (2003).
- [4] *Metamaterial Structures, Phenomena, and Applications*, edited by T. Itoh and A. A. Oliner, special issue of IEEE Trans. Microwave Theory Tech. **53**(4), (2005).
- [5] N. Engheta and R. W. Ziolkowski, IEEE Trans. Microwave Theory Tech. **53**, 1535 (2005).
- [6] *Metamaterials*, special issue of J. Opt. Soc. Am. B **23**(3) (2006), edited by A. Boardman and V. Shalaev.
- [7] N. Engheta, IEEE Antennas Wireless Propag. Lett. **1**, 10 (2002).
- [8] G. Shvets, Phys. Rev. B **67**, 035109 (2003).
- [9] S. Enoch, G. Tayeb P. Sabouroux, N. Guerin, and P. Vincent, Phys. Rev. Lett. **89**, 213902 (2002).
- [10] A. Alù, and N. Engheta, Phys. Rev. E **72**, 016623 (2005).
- [11] M. Silveirinha and N. Engheta, Phys. Rev. Lett. **97**, 157403 (2006).
- [12] J. Gómez Rivas, C. Janke, P. Bolivar, and H. Kurz, Opt. Express **13**, 847 (2005).
- [13] W. Rotman, IRE Trans. Antennas Propag. **10**, 82 (1962).
- [14] J. B. Pendry, A. J. Holden, W. J. Stewart, and I. Youngs, Phys. Rev. Lett. **76**, 4773 (1996).
- [15] M. Silveirinha and C. A. Fernandes, IEEE Trans. Microwave Theory Tech. **53**, 1418 (2005).
- [16] D. Schurig, J. J. Mock, and D. R. Smith, Appl. Phys. Lett. **88**, 041109 (2006).
- [17] J. B. Pendry, D. Schurig, and D. R. Smith, Science **312**, 1780 (2006).
- [18] U. Leonhardt, Science **312**, 1777 (2006).
- [19] U. Leonhardt, New J. Phys. **8**, 118 (2006).
- [20] S. A. Cummer, B. I. Popa, D. Schurig, D. R. Smith, and J. Pendry, Phys. Rev. E **74**, 036621 (2006).
- [21] D. Schurig, J. J. Mock, B. J. Justice, S. A. Cummer, J. B. Pendry, A. F. Starr, D. R. Smith, Science **314**, 977 (2006).
- [22] N. A. Nicorovici, R. C. McPhedran, and G. W. Milton, Phys. Rev. B **49**, 8479 (1994).
- [23] G. W. Milton and N. A. P. Nicorovici, Proc. R. Soc. London, Ser. A **462**, 3027 (2006).
- [24] P. S. Kildal, A. A. Kishk, and A. Tengs, IEEE Trans. Antennas Propag. **44**, 1509 (1996).
- [25] R. Marqués, J. Martel, F. Mesa, and F. Medina, Phys. Rev. Lett. **89**, 183901 (2002).
- [26] S. Hrabar, J. Bartolic, and Z. Sipus, IEEE Trans. Antennas Propag. **53**, 110 (2005).
- [27] Robert E. Collin, *Field Theory of Guided Waves*, 2nd ed. (IEEE Press, New York, 1991), pp. 664–671.
- [28] V. Agranovich and V. Ginzburg, *Spatial Dispersion in Crystal Optics and the Theory of Excitons* (Wiley-Interscience, New York, 1966).
- [29] P. A. Belov, R. Marqués, S. I. Maslovski, I. S. Nefedov, M. Silveirinha, C. R. Simovski, and S. A. Tretyakov, Phys. Rev. B **67**, 113103 (2003).
- [30] A. Alù and N. Engheta, IEEE Trans. Antennas Propag. **51**, 2558 (2003).
- [31] J. F. Carlson and A. E. Heins, Q. Appl. Math. **4**, 313 (1947).
- [32] J. F. Carlson and A. E. Heins, Q. Appl. Math. **5**, 82 (1947).
- [33] C. R. Simovski, S. A. Tretyakov, A. H. Sihvola, and M. M. Popov, Eur. Phys. J.: Appl. Phys. **9**, 195 (2000).
- [34] C. R. Simovski and B. Sauviac, Eur. Phys. J.: Appl. Phys. **17**, 11 (2002).
- [35] M. Silveirinha, IEEE Trans. Antennas Propag. **54**, 1766 (2006).
- [36] C. P. Wu and V. Galindo, IEEE Trans. Antennas Propag. **14**, 163 (1966).
- [37] For large objects, the multipoles contributing to the scattering become many in number and therefore this technique may not provide sufficient degrees of freedom to suppress all of them simultaneously. We are currently working on ideas to extend these concepts to objects with physical cross sections of several wavelengths.
- [38] A. Alù and N. Engheta, J. Appl. Phys. **97**, 094310 (2005).
- [39] Xiaoming Zhou and Gengkai Hu, Phys. Rev. E **74**, 026607 (2006).
- [40] CST Microwave Studio™ 5.0, CST of America, Inc., URL: www.cst.com